L. Daniel Maxim
Leigh Harrington
Everest Consulting Associates
Princeton Junction, NJ 08550

"Scale-Up" Estimators for Aerial Surveys with Size-Dependent Detection

The parametric size-dependent approach, though requiring considerable mathematical manipulation, has the ability to extract the maximum information from limited amounts of ground truth data.

Introduction

In many aerial surveys the population of items being studied varies considerably in size. This is true, for example, in agricultural crop surveys where the size of agricultural fields varies among farms (Podwysocki, 1976; Bauer *et al.*, 1979), in forestry surveys designed to detect and measure human disturbances and insect infestation (Aldrich 1975; Ashley, 1979; Bernstein, 1974), and in wildlife management surveys to determine the number and size of ponds and lakes available to breeding waterfowl (Work and Gilmer, 1976; Gilmer *et al.*, 1978), to cite some specific examples. If the smallest items in the population are beneath the detection capability of the camera/film/platform being employed, then they cannot be observed or measured. Even items above this threshold may not be detected with certainty. For example, in the aerial survey conducted by Bernstein (1974) to identify individual trees in a reforestation project, photo interpreters (PIs) failed to detect between 50 percent to 75 percent of all trees in the test area, even at a scale of 1:1000. In the study of spruce budworm damage (Ashley, 1979) it was noted that, as the scale was decreased from 1:63,000 to 1:31,600 to 1:15,800 and, finally, to 1:10,600, the number of detected dead trees/block increased, on average from 1.84 to 2.66, 7.91, and 10.75, respectively. As a second example, data of Roswell (cited in Estes *et al.*, 1975) have shown that the detectability of lakes on radar images is "a complex function of the system(s), look angle, topography, and size of lake." However, detectability was primarily a function of size and secondarily of environment. In one series of experiments, detection probabilities were about 0.25 for lakes ranging in size from 0 to 2 acres and 0.80 or more for lakes larger than 30 acres.

Abstract: *A general discussion of the problem of size-dependent detection in aerial surveys is presented. Three basic analytical approaches for creating models of size-dependent detection are outlined together with their advantages and disadvantages. One of these approaches, using parametric population and detection models, is explored in some detail. Formulae are presented for a variety of population size distributions and alternative detection functions. In particular, the inverse gaussian size distribution and extreme value detection function are proposed as being realistic, flexible, and analytically tractable. Appropriate formulae are developed for this model and are illustrated with examples from the literature.*

Generally the detection probability increases with the size of the objects or with increased resolution of the observation system. (At the opposite extreme, the largest members of the population might not be recognized if they exceeded the size of the image frame. Even if detected, they cannot be fully measured unless adjacent quadrats are also imaged. This problem is self evident and will not be discussed further.) If a significant number of items are missed due to size-dependent effects, statistical models need to be employed to produce accurate estimates.

To avoid an excessively abstract presentation,

Photogrammetric Engineering and Remote Sensing,
Vol. 48, No. 8, August 1982, pp. 1271-1287.

0099-1112/82/4808-1271$02.25/0

consider the specific case of a survey designed to estimate the hectareage of some crop under cultivation in a given region. The resulting imagery-derived data require several adjustments. A "scale-up" factor is needed to estimate total fields or hectareage if the survey included only a sample rather than a complete census of the population. Additional adjustments may be required to correct for detection/misclassification errors as shown in Maxim *et al.* (1981a, 1981b, 1981c). In a broadly similar fashion, the bias introduced by size-dependent detection can be estimated and removed. Because it is assumed in this paper that smaller fields are more difficult to detect than those that are larger, the average size of the fields that are detected from the imagery is always greater than the true average field size. Further (assuming no false positives or misclassification errors), the number of fields detected in the imagery is always less than the true number present. However, depending on the nature of the size dependence, the total area of fields detected, while always less than the true amount, may be nearly correct. This is because this area is obtained as a product of the number of fields detected (an underestimate) and the average field size of those detected (an overestimate).

Scope

Three alternative approaches that illustrate the main concepts and requisite methodologies needed to analyze data from an aerial survey in the presence of size-dependent detection are presented. (Landsat or similar imagery will require additional correction. For imagery of this type, not only are fields "missed" when they are too small (a Landsat pixel represents about 1.1 acres) but also the estimated size (i.e., number of pixels) of the fields detected is a discrete random variable. That is, even assuming perfect classification of the "pure" pixels, the true size can be under- or over-estimated simply due to the orientation of the platform with regard to the target. See the work of Cropper (1980) for useful background.)

The results developed here assume that *there are no significant misclassification errors* or, if these errors do occur, that they are not functionally related to the size of the fields and thus can be accounted for separately (see Maxim *et al.* (1981c) for an exposition). If detection and classification are independent processes, then this assumption holds exactly. If the linkage between these processes is weak, then the results are approximately correct. In cases where the linkage is strong, as for example where size itself is one of the arguments in a discriminant analysis function, modifications need to be made to the models presented here. Though these modifications serve to complicate the analysis, the necessary theoretical development parallels that given in this paper.

Size Dependent Detection Models

To analyze data in cases where detection is a function of size, two approaches are immediately evident. The first, and, from a reading of the literature, the most common, is to reflect the size dependence only implicitly in an overall detection probability that is used for scaling-up results. This approach is valid if the ground truth sample is a *random sample* of the area imaged, and there is no relationship between field size and location within the stratum being sampled. Under these circumstances the estimated detection probability correctly reflects the size distribution of the population. But often a truly random ground truth sample is difficult or expensive to obtain. Moreover, as the observed detection probability depends upon the size distribution of the fields, periodic recalibration is necessary to guard against shifts in the size distribution and, therefore, the resulting detection probability. An aerial survey of ponds as waterfowl habitat, for example, has to cope with population size shifts associated with both seasonal and cyclical rainfall patterns. Likewise, a study of agriculture in developing countries might encounter temporal size trends reflecting the introduction of new agricultural methods, land reform and redistribution, and other factors. Table 1 contains hypothetical data from an imagery experiment that illustrates the above points. The first four columns show illustrative size ranges, the number of fields in the ground truth sample of the population, the true (but unknown) detection probability for fields in each of the size ranges, and the expected number of these fields that would be discovered in a matched ground truth and imagery experiment. According to these data for Case A, of a total of 1000 fields in the ground truth sample, the expected number detected would be 520 or 52 percent, i.e., the *overall* field detection probability is 0.52. Given the approach under discussion, 0.52 would be used for scaling-up observed quadrat field counts; e.g., if 250 fields were observed in other quadrats in the survey then 250/0.52 or 481 fields would be estimated. See Maxim *et al.* (1981c) for additional details. Note also that the fraction of the total area detected (using the mid-point of the size range in each category as representative of the size of all fields in that category, a slight inaccuracy) for case A is 0.608. In general this quantity will exceed the fraction of fields detected whenever the detection probability increases with size.

But now suppose that the ground truth sample is not representative of the population or alternatively that, over time, the population shifts to that shown as case B of table 1. The true overall detection probability for this case is 0.395, not 0.52 as before, and the resulting scale-up factor is likewise altered. This example shows the impor-

TABLE 1. HYPOTHETICAL DATA FROM AN IMAGERY EXPERIMENT

Field Size x, Arbitrary Units	Number of Fields of this Size in Ground Truth Sample	True Detection Probability for Fields of this Size	Expected Number Detected	Approximate Average Field Size in this Class	Expected Area Detected
Case A:					
$1 \leq x < 2$	400	0.3	120	1.5	180
$2 \leq x < 3$	300	0.5	150	2.5	375
$3 \leq x < 4$	200	0.8	160	3.5	560
$4 \leq x < 5$	100	0.9	90	4.5	405
All	1000	N/A	520	Total Area 2500	1520
		Fraction Total Fields	0.520	Fraction Total Area	0.608
Case B:					
$1 \leq x < 2$	700	0.3	210	1.5	315
$2 \leq x < 3$	200	0.5	100	2.5	250
$3 \leq x < 4$	50	0.8	40	3.5	140
$4 \leq x < 5$	50	0.9	45	4.5	202.5
Total	1000	N/A	395	Total Area 1950	907.5
		Fraction Total Fields	0.395	Fraction Total Area	0.465

tance of a random sample and a constant population if this method is being employed. The work of Gilmer *et al.* (1980) represents an interesting variant on this idea using a regression estimate. However, space constraints do not permit discussion of this paper here.

An alternative to simple scaling is to stratify the population into several size categories, such that the detection probability within each stratum is approximately constant, much as was done in Table 1. A detection probability can then be estimated for each size stratum. Scale-up methods (described later) are then used to correct for the observed size dependence. The advantage of this technique is that the ground truth sample need not be a random sample of the field size population but can be gathered at whatever locations are convenient, provided that the fields surveyed span the entire size range and are otherwise representative with respect to identification/detection. The disadvantage of this stratified procedure is that the required size of the ground truth sample is much larger than if the simple scale-up approach were used. However, because separate scale-up factors are developed for each size range, shifts in the population size distribution do not result in biased estimates of population totals. Returning to the data given in Table 1, for example, note that this second approach would measure the detection probabilities in each size range, i.e., the quantities shown in column 3. The scale-up rules are applied *for fields in each size range* rather than on an aggregated basis. Thus, if 210 fields of size $1 \leq x < 2$ are discovered in the sample, then the estimated number of fields in this size range is 210/0.3 or 700, etc., and the estimated total number of fields is the sum of the estimated number of fields in each size range. No assumption of randomness (of size) of ground truth fields is required and the procedure is robust to population shifts. But, because many more detection probabilities need to be estimated, the size of the calibration sample is larger than for the first approach. These two methodologies are summarized in Table 2.

Shown also in Table 2 is a third approach, denoted *parametric size-dependent detection.* Figure 1 gives additional details. Here it is assumed that the size of fields within the region of interest (stratified if necessary) varies according to some explicit distribution, denoted $f(x|\theta)$, and termed the 'parent distribution.' Practical choices for a parent distribution include the log-normal, gamma (including the exponential and chi square), inverse gaussian, Weibull, and the Pareto distributions. The Pareto, for example, is often used to model the size of craters on the moon and other planets (Hartman, 1977). More generally, any distribution that does not assign probability to negative sizes is admissible; though, of course, it must fit the population data to be useful.

In addition to the parent distribution, a detection function, denoted $D(x|\psi)$, is required to specify the dependence of detection probability upon field size, x. It is assumed here that this function is monotone non-decreasing between 0 and 1. That is, the larger the field, the greater the probability of detection and, further, very large fields are virtually certain to be detected. This latter assumption is easily relaxed by multiplying the detection function by a quantity, γ, $0 < \gamma \leq 1.0$ to accommodate the non size-dependent portion of the detection process. (Detection probabilities are likely to be a function of many factors in addition to size, e.g., platform, film, season, terrain, location of objects, etc. These effects are subsumed in the term γ.) Likewise, functions having values greater

TABLE 2. DETECTION MODELS

Model	Description	Advantages	Disadvantages	Remarks
"Simple Scale Up"	A detection probability is calculated without regard to size using a ground truth sample to determine fraction of fields/area missed. Alternatively, capture-recapture methods can be employed.	Uncomplicated analysis and modest sample size is needed for ground truth.	The ground truth sample needs to be a random sample from the total area to be surveyed; a requirement sometimes difficult, costly, or impossible to satisfy.	For a one time survey, this is an effective and inexpensive approach. The scale up factor, however, needs to be re-estimated whenever the population or detection methodology changes.
Discrete Size Dependent Detection (a non-parametric approach)	Fields are divided into several size categories. Within each size class, the detection probability is assumed constant. This probability is estimated using ground truth data.	Reasonably straightforward analysis. Requires no distributional assumptions about population, nor is a randomness assumption needed for ground truth sample.	This procedure needs a large ground truth sample, increasing with the number of categories defined.	If a significant fraction of the population is below the resolution of the system, the "Simple Scale Up" methodology may be required for this stratum. This would reduce the usefulness of the model.
Parametric Size Dependent Detection	Both the population distribution of field sizes and the size dependent detection mechanism are modeled. Either or both may have to be estimated from a ground truth sample or survey data.	Ground truth requirements are more flexible and varied and in certain circumstances are not required at all. Several variables, in addition to field size, can be easily incorporated into the detection model.	Mathematically, the analysis can sometimes be extremely complicated, requiring a computer to solve. The resulting estimates may have large uncertainties, depending upon the quality of the ground truth.	This model relaxes ground truth requirements at the expense of mathematical sophistication.

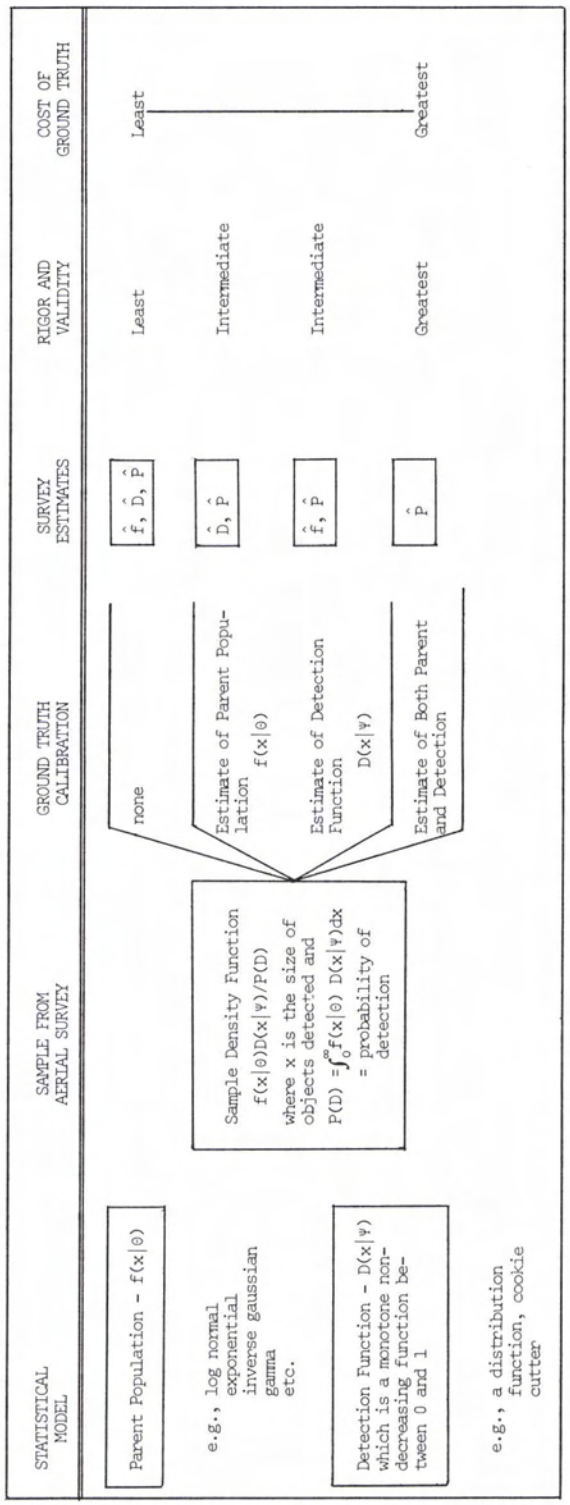

FIG. 1. An anatomy of size-dependent detection for an aerial survey.

than 1.0 can be allowed with some adjustments to interpretation as an artifice to model false positives. With these conventions, all detection functions are distribution functions. A special case of practical interest is the so-called "cookie cutter" detection function. The cookie cutter assumes that all fields below a threshold size value, denoted by the symbol c, are not detected, whereas those above c are always detected.

Taken together, the parent population and the detection function define the distribution of those fields that are discovered in the imagery. In particular, the density function of the size of discovered fields is given by the expression,

$$g(x|\theta, \psi) = f(x|\theta)\, D(x|\psi)/P(D), \qquad (1)$$

where $P(D)$ is the overall fraction of fields detected and is equal to

$$P(D) = \int_0^\infty f(x|\theta)\, D(x|\psi)dx. \qquad (2)$$

Figure 2 shows an example where both the parent density and detection functions are exponential distributions. Note that the size distribution of fields observed in the imagery is very different from that assumed for the parent; both the shape of the distribution and the various moments differ. This case is considered in greater detail in a later section.

As is implied by Figure 1, it may be possible to estimate the unknown parameters θ and ψ without the benefit of a ground truth sample. This is done by varying the assumed parameters of the parent population and detection function until a close match is obtained between the observed field size distribution (i.e., that determined from imagery) and that calculated from the model. However, depending upon the distribution and the detection functions, one or more parameters may not be estimable (see discussion of the inverse gaussian model). And even if all parameters can be estimated uniquely, they may have large uncertainty. Thus, some form of ground truth is often required, if only to validate the model.

Ground truth requirements for the parametric size-dependent detection model, however, are typically more flexible than those needed for the other procedures shown in Table 2. The simplest approach is to estimate the detection function directly; imagery from an area of known ground truth is interpreted and the correspondence between detection and size is noted. The detection function can be fitted and tested from these data (see Cox (1970) or Maxim (1973) for a résumé of appropriate procedures). This same experiment can be used to measure the non size-dependent component of the detection probability. Alternatively, a ground truth sample can be designed to estimate the parent population function $f(x|\theta)$. Given knowledge of either the parent population or the detection function, the remaining parame-

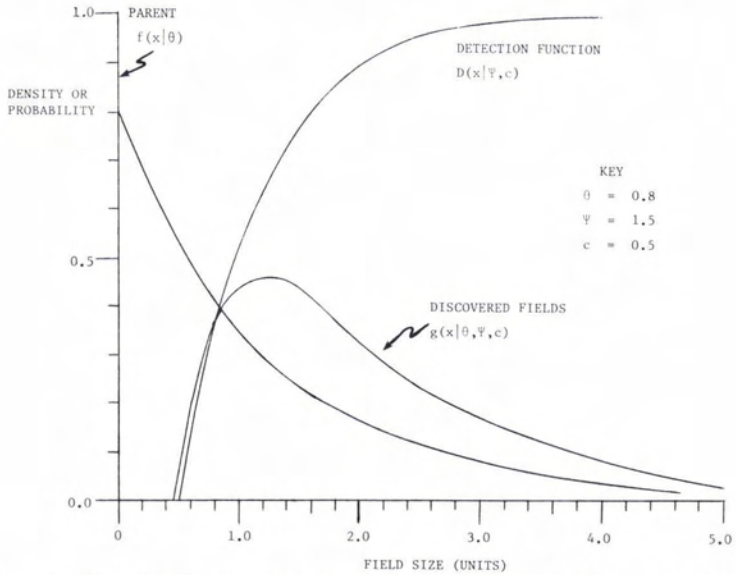

FIG. 2. The density function for an aerial survey sample having size-dependent detection.

ters in the model can be efficiently estimated from the aerial survey data. Note that a random ground truth sample is not required to estimate $D(x|\psi)$, but is required to estimate $f(x|\theta)$. But estimation of $D(x|\psi)$ ordinarily requires both ground and imagery acquisition and interpretation of matching ground truth fields, typically a time consuming process. (One of the reviewers suggested an intriguing alternative: acquire, on the same sortie, imagery at two or more scales, one of which may be satisfactory as "ground truth.") Other types of ground truth collection can also be utilized to reflect the particular circumstances of an aerial survey. It may be possible to establish the parent density function from a totally different source, for example, from statistics kept by a local, state, or federal government agency. This approach is illustrated in an example given in the next-to-last section. Such exogenous information can reduce the cost of the survey substantially.

The balance of this paper is devoted to an exploration of parametric size-dependent detection models. Beginning with the simple case of an exponential parent/cookie cutter detection model, the discussion covers successively more general models for analysis.

Cookie Cutter Detection with Exponential Parent

One of the simplest cases that can be considered is where the parent distribution is exponential, i.e., given by

$$f(x|\theta) = \theta e^{-\theta x} \tag{3}$$

and the detection function is simply a cookie cutter with a threshold equal to c. For this case it can be shown that the density function of the size of those fields detected in the aerial survey is also exponential, but shifted to the right by an amount equal to the threshold. That is,

$$g(x|\theta,c) = \begin{cases} 0 & x \leq c \\ \theta e^{-\theta(x-c)} & x \geq c. \end{cases} \tag{4}$$

Figure 3 summarizes the pertinent analytical results for this case.

In particular, the detection probability is

$$P(D) = e^{-\theta c}, \tag{5}$$

and the average size of those fields detected is $1/\theta + c$; i.e., the average field size of the parent distribution shifted to the right by c. To illustrate, suppose the mean field size were 0.05 hectares (ha) and that the detection threshold were 0.03 ha. (i.e., $\theta = 1/0.05$ and $c = 0.03$). The detection probability calculated from Equation 5 is 0.549, and the average size of fields detected in the imagery would be 0.08 ha. If the size dependence had either been ignored or remained unrecognized, then the true number, N, of fields in the imagery would have been underestimated as

$$\begin{aligned} \text{number of fields detected} &= N \cdot P(D) \\ &= Ne^{-\theta c}, \end{aligned} \tag{6}$$

or only about 55 percent of the true number in this example, while the total area of the fields detected would have been calculated as

$$\begin{aligned} \text{total area detected} &= N \cdot P(D) \cdot (\text{ave. field size}) \\ &= Ne^{-\theta c}(1/\theta + c), \end{aligned} \tag{7}$$

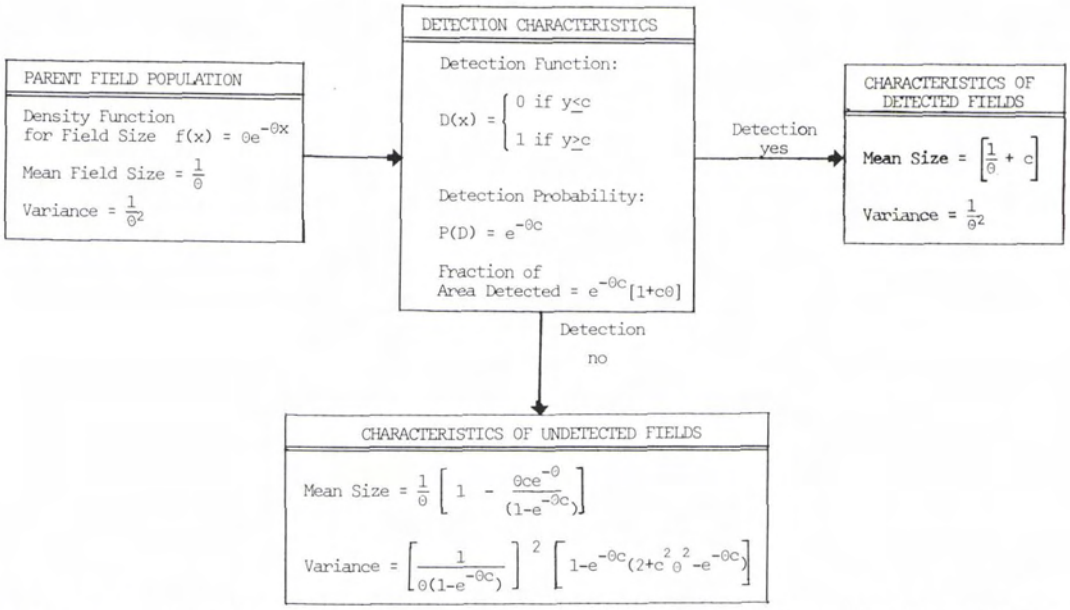

FIG. 3. Summary of analytical results for a simple example: exponential field size and "cookie cutter" detection.

or about 88 percent of the true area. It is easily shown that this value is always less than N/θ, the actual total area in the imagery. Table 3 shows calculations of the bias for a range of values of the product θc. Note that, when the value of θc is 0.25 or less, the area underestimate can be quite small even though as many as 20 percent of the fields are not detected. These are circumstances where modeling size-dependent detection produces only a small benefit in terms of increased accuracy.

If no ground truth is available, the maximum likelihood estimates of c and θ are

$$\hat{c} = \min(x_1, x_2, \ldots, x_n), \tag{8}$$

$$\hat{\theta} = 1/(\bar{x} - \hat{c}), \text{ where } \bar{x} = \sum x_i/n. \tag{9}$$

Other estimators are given in Johnson and Kotz (1970), depending upon what additional assumptions can be made about c and θ. Table 4 shows results for other parent distributions assuming cookie cutter detection.

Exponential Detection with Exponential Parent

This case is graphically illustrated in Figure 2. The detection function for this model is

$$D(x|\psi,c) = \begin{cases} 1 - e^{-\psi(x-c)} & x \geq c, \\ 0 & x \leq c. \end{cases} \tag{10}$$

This detection function is analytically quite simple; it often provides a useful approximation in practice. For example, with minor modification to account for non size-dependent effects, this model provides an excellent fit to the aforementioned Roswell data (cited in Estes *et al.* (1975)) for detection of lakes from radar imagery. As with the cookie cutter model, it has the characteristic that below a threshold value, c, no fields are detected. However, above the detection threshold, the probability of detection increases only gradually with size, as given in Equation 10. As ψ gets large, this detection function approaches a cookie cutter.

TABLE 3. THE BIAS AND DETECTION PROBABILITY FOR EXPONENTIAL PARENT AND COOKIE CUTTER DETECTION

	The Value of θc									
	0.0625	0.125	0.25	0.5	0.6	1	2	4	8	16
Bias (fraction of area detected)	0.998	0.993	0.974	0.910	0.878	0.736	0.406	0.091	0.003	1.9×10^{-6}
Probability of detection (fraction of fields detected)	0.939	0.882	0.779	0.607	0.549[1]	0.368	0.135	0.018	0.0003	1.1×10^{-7}

[1] Example in text.

TABLE 4. COOKIE CUTTER DETECTION FOR VARIOUS PARENT DISTRIBUTIONS: A USEFUL RESUME OF FORMULAE

Name	Density Function $f(x\|\theta)$	Size Distribution of Detected Fields $x > c$, $g(x\|\theta,c)$
Exponential	$\theta e^{-\theta x}$	$\theta e^{-\theta(x-c)} x \geq c$
Pareto	$\frac{ak^a}{x^{a+1}} \; x \geq k \quad c \geq k$	$\frac{ac^a}{x^{a+1}} \; x \geq c$
Rayleigh (Weibull with with $\beta = 2$)	$\theta \cdot x \cdot \exp\left\{\frac{-\theta x^2}{2}\right\}$	$\theta \cdot x \cdot \exp\left\{-\frac{\theta}{2}(x^2 - c^2)\right\}$ $x \geq c$
Weibull	$\beta/a\left(\frac{x}{a}\right)^{\beta-1} \exp\left\{-\left(\frac{x}{a}\right)^{\beta}\right\}$	$\beta/a\left(\frac{x}{a}\right)^{\beta-1} \exp\left(-\left(\frac{x}{a}\right)^{\beta} + \left(\frac{c}{a}\right)^{\beta}\right)$ $x \geq c$
Inverse Gaussian	$\left(\frac{\mu\phi}{2\pi x^3}\right)^{1/2} \exp\left(\frac{-\phi x}{2\mu} + \phi - \frac{\mu\phi}{2x}\right)$	$f(x)/P(D)$ $x \geq c$

$\Gamma(a+1, c) = \int_c^{\infty} x^a \exp^{-x} dx$ = incomplete gamma function

Figure 4 summarizes the characteristics of this model. To illustrate, suppose that $\theta = 1/0.05$ and $c = 0.03$ as in the first numerical example, but now assume that the detection function is exponential with $\psi = 20$. Given these assumptions, the fraction of fields detected is 0.27 and the fraction of area detected is 0.58, values calculated from the equations given in Figure 4.

Estimating the parameters of this model is more difficult than for the cookie cutter version. If all three parameters must be estimated from the aerial survey data alone, then the method of maximum likelihood can be used. That is, the likelihood function below is maximized:

$$L = \prod_{i=1}^{n} g(x_i|c,\theta,\psi), \tag{11}$$

with respect to $c > 0$, $\theta > 0$, $\psi > 0$. The resulting differential equations do not simplify appreciably, and in this case a numerical search procedure must be used to find the maximizing values.

If the value of c is known or is to be estimated as the smallest field detected in the imagery, then the method of moments can be used as an alternative to maximum likelihood. This is done by setting the sample moments (e.g., the mean and variance) equal to their population values as given in Figure 4. Solving the two resulting equations gives the following estimates:

$$\hat{\theta} = \frac{\bar{x} - c - (2s^2 - (\bar{x} - c)^2)^{1/2}}{(\bar{x} - c)^2 - s^2} \tag{12}$$

and

$$\hat{\psi} = \frac{2}{((\bar{x} - c)^2 - s^2)\hat{\theta}} - \hat{\theta} \tag{13}$$

where $\bar{x}$ and s^2 are the average field size and the sample variance of those fields detected in the imagery. For example, if $\bar{x}$ were 0.10, s^2 were 0.0030, and c were known to be 0.03, then from Equations 12 and 13 the resulting estimates of $\hat{\theta}$ and $\hat{\psi}$ would be 19.39 and 34.9, respectively. Note the sensitivity of these estimates to the values of $\bar{x}$, s^2, and c. This example was developed by rounding the values of $\bar{x}$ and s^2 from the values computed assuming $\theta = 20$ and $\psi = 20$ used earlier (i.e., letting $\bar{x} = 0.1$ rather than 0.105 and $s^2 = 0.0030$ rather than 0.003125); while $\hat{\theta}$ is quite similar, $\hat{\psi}$ has nearly doubled. Note also that these equations may lead

TABLE 4. *Continued*

Mean Size of Detected Fields, U^*	Fraction of Fields Detected $P(D)$	Fraction of Area Detected $P(D)\ \mu^*/\mu$
$1/\theta + c$	$c^{-\theta c}$	$e^{-\theta c}[1 + \theta c]$
$\frac{ac}{a-1}$ $a > 1$ ∞ $a \leq 1$	$\left(\frac{k}{c}\right)^a$	$\left(\frac{k}{c}\right)^{a-1}$ $a \geq 1$ 1 $a \leq 1$
$\left(\frac{2}{\theta}\right)^{1/2} \exp\left(\frac{\theta c^2}{2}\right) \Gamma\left(3/2, \frac{c^2\theta}{2}\right)$	$\exp(-\theta c^2/2)$	$\frac{\Gamma\left(3/2, \frac{c^2\theta}{2}\right)}{\Gamma(3/2)}$
$a \cdot \exp(c/a)^\beta \Gamma\left(1 + 1/\beta, \left(\frac{c}{a}\right)^\beta\right)$	$\exp\left(-\left(\frac{c}{a}\right)^\beta\right)$	$\frac{\Gamma\left(1 + 1/\beta, \left(\frac{c}{a}\right)^\beta\right)}{\Gamma(1 + 1/\beta)}$
$\mu^* = \int_c^\infty xf(x)/P(D)$	$1 - \Phi\left(\left(\frac{c}{\mu} - 1\right)\left(\frac{\mu\phi}{c}\right)^{1/2}\right)$ $-e^{2\phi}\Phi\left(-\left(\frac{c}{\mu} + 1\right)\left(\frac{\mu\phi}{c}\right)^{1/2}\right)$	$\frac{P(D)\mu^*}{\mu}$

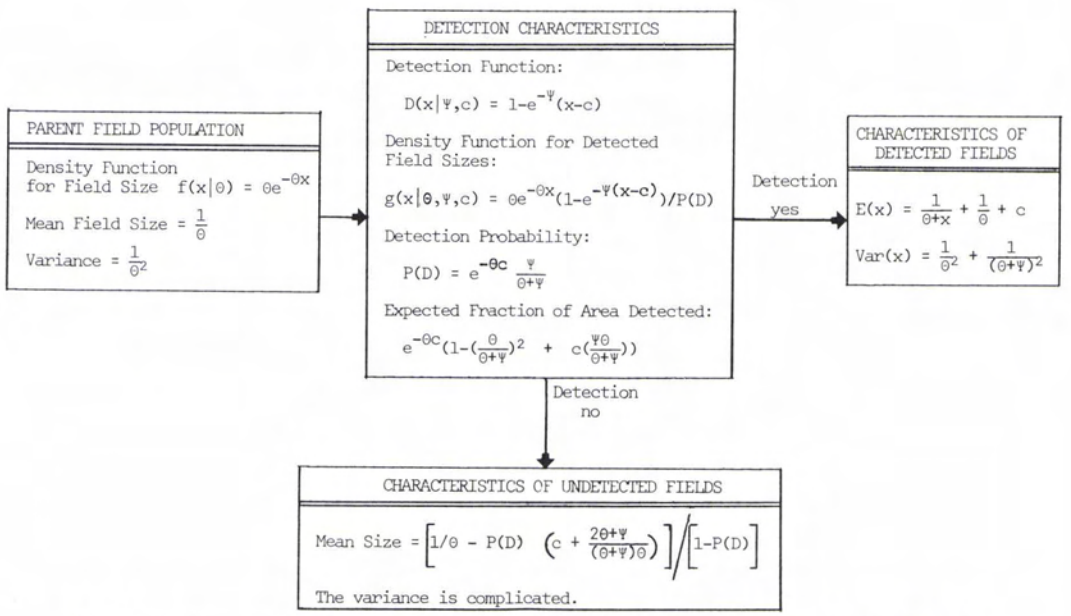

FIG. 4. Summary of analytical results: exponential field size with exponential detection.

to negative estimates. In fact, in order for $\hat{\theta}$ to be positive and real, it is necessary that

$$1/2(\bar{x} - c)^2 < s^2 < (\bar{x} - c)^2 \qquad (14)$$

is satisfied by the data. Thus, the estimates given by Equations 12 and 13 above may not be applicable in all cases, and, further, may require a substantial amount of data in order to estimate the parameters with any precision.

If ground truth and matching imagery are collected to determine which fields are missed in the aerial survey, then this information can be used to estimate ψ and c, the parameters associated with the detection function, $D(x|\psi,c)$. Maximum likelihood estimates of these parameters can be obtained analytically or numerically. An alternative approach is given below.

The fields in a ground truth sample are stratified into N size categories with mid points, x_i, such that the detection probability is essentially constant within each stratum. Denote $\hat{P}_i$ as the observed fraction of fields detected in the i^{th} stratum and n_i the associated sample size. Reorganizing Equation 10 yields the predicted detection probability for the ith stratum, P_i, as

$$\ln(1 - P_i) = -\psi(x_i - c). \qquad (15)$$

That is, the unknown parameters ψ and c are linear in $\ln(1 - P_i)$ and can be estimated by least-squares procedures. An improvement (q.v., Berkson, (1955)) is the use of weighted least squares, where the weights are proportional to the inverse of the variance of $\ln(1 - \hat{P}_i)$. For large samples this variance is equal to $P/(1 - P)n$, and so ψ and c are estimated by minimizing the expression

$$\sum_{i=1}^{N} \frac{n_i(1 - \hat{P}_i)}{\hat{P}_i} (\ln(1 - \hat{P}_i) + \psi(x_i - c))^2, \qquad (16)$$

or equivalently, by obtaining the weighted least-squares regression estimates for ψ and c. Berkson shows, in a similar situation, that the above estimates have the same large sample properties as the maximum likelihood estimates and can actually be better (smaller mean squared error) in small samples. The principal limitation to the above approach is that, with a small total sample size, it is not possible to define strata with essentially a uniform detection probability and also have a large enough sample size, n_i, to estimate P_i with precision. In practice, then, it may be necessary to combine neighboring strata so as to increase this sample size even though the resulting estimates will now be biased. For small sample sizes, a maximum likelihood treatment such as illustrated in the appendix may offer a better estimator than the regression model advanced above.

The Inverse Gaussian Distribution: Candidate for a Parent

The ease of computation associated with the exponential parent, as demonstrated in the previous sections, is an attractive attribute of this model. Unfortunately, for many potential applications, the appropriate parent distribution is better described by a log-normal, gamma, or Poisson distribution. For these distributions, numerical methods are required to analyze data having size dependent detection. The inverse gaussian distribution, given below, is an important exception to this rule; i.e.,

$$f(x|\mu\phi) = \left(\frac{\mu\phi}{2\pi x^3}\right)^{1/2} \exp\left(\frac{-\phi x}{2\mu} + \phi - \frac{\mu\phi}{2x}\right). \qquad (17)$$

Since this distribution is not well known, this section will present some of its important properties. For additional details see Tweedie (1957a, 1957b) or Johnson and Kotz (1970). Table 4 provides a useful résumé of formulae for this distribution. The important point to be made here is that the distribution is flexible (able to aproximate many real world size distributions) and is analytically tractable. Figure 5 gives representative curves from this distribution for various values of $\lambda = \mu\phi$ and unit expectation. Note that as λ becomes large, the inverse gaussian approaches the normal distribution, whereas for smaller values of λ the distribution is more skewed and resembles a log-normal or Weibull.

Because, for small values of x, the density function Equation 17 is dominated by the term $\mu\phi/2x$ in the exponential, while for large values of x, it is dominated by the $\phi x/\mu$ term, both the right and left tails of an empirical distribution can often be fitted well by an inverse gaussian. The applicability of this model to the size distribution of agricultural fields is illustrated in a later section.

The Extreme Value Detection Distribution with Inverse Gaussian Parent

A detection function that analytically complements the inverse gaussian parent is the so-called extreme value distribution. It is given by

$$D(x|\psi) = e^{-\psi/x} \quad x \geq 0. \qquad (18)$$

(This function can be easily modified to account for threshold effects. This is omitted in the interest of computational simplicity in what follows). The appendix shows how maximum likelihood estimates of the parameter ψ can be computed from observed detection results, while Figure 6 illustrates this function graphically for various values of ψ. The appendix also provides the equations for maximum likelihood estimates of this model if a non size-dependent term is included.

TABLE 5. A RESUME OF USEFUL FORMULAE FOR THE INVERSE GAUSSIAN DISTRIBUTION

Item	Formula
Density Function	$f(x\|\mu\phi) = (\mu\phi/2\pi x^3)^{1/2} \exp\left\{\frac{-\phi x}{2\mu} + \phi\frac{-\mu\phi}{2x}\right\}$ $x > 0$
Distribution Function	$F(x) = \Phi\left(\left(\frac{x}{\mu} - 1\right)\left(\frac{\mu\phi}{x}\right)^{1/2}\right) + e^{2\phi}\,\Phi\left(-\left(\frac{x}{\mu} + 1\right)\left(\frac{\mu\phi}{x}\right)^{1/2}\right)$ where Φ = standard normal integral available from tables
Mean	$E[x] = \mu$
Variance	$\mathrm{Var}[x] = \mu^2/\phi$
Mode	$x_{\text{mode}} = \mu\left((1 + 9/4\phi^2)^{1/2} - 3/2\phi\right)$
Maximum Likelihood Estimates (where $\lambda = \mu\phi$)	$\hat{\mu} = \bar{x} = \sum x_i/n$ $\hat{\lambda} = \left(\sum(1/x_i)/n - 1/\bar{x}\right)^{-1}$
Skewness	$\sqrt{\beta_1} = 3\sqrt{\mu/\lambda}$ (= 0 for normal distribution)
Kurtosis	$\beta_2 = 3 + 15\,\mu/\lambda$ (=3 for normal distribution)

The analytical convenience and simplicity of this detection function arises from the property that if the parent is inverse gaussian, then so, too, is the theoretical distribution of detected fields from the aerial survey. (The proof of this assertion is straightforward and is omitted). Analytical results are summarized in Figure 7.

The parameters of the distribution of discovered fields denoted by μ^* and ϕ^* are directly calculable from the parameters of the parent distribution and the detection function as

$$\mu^* = \left(\mu(2\psi + \mu\phi)/\phi\right)^{1/2} \tag{19}$$

and

$$\phi^* = \left(\phi(2\psi + \mu\phi)/\mu\right)^{1/2}, \tag{20}$$

and the fraction of fields detected is given by

$$P(D) = (\mu\phi/(2\psi + \mu\phi))^{1/2} \exp\left\{\phi - (\phi(2\psi + \mu\phi)/\mu)^{1/2}\right\}. \tag{21}$$

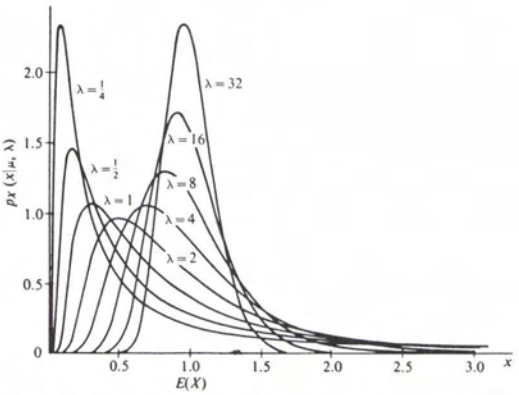

FIG. 5. Inverse gaussian distributions all having E(x) = 1.0 (=μ) where $\lambda = \mu\phi$ (taken from Tweedie (1975a)).

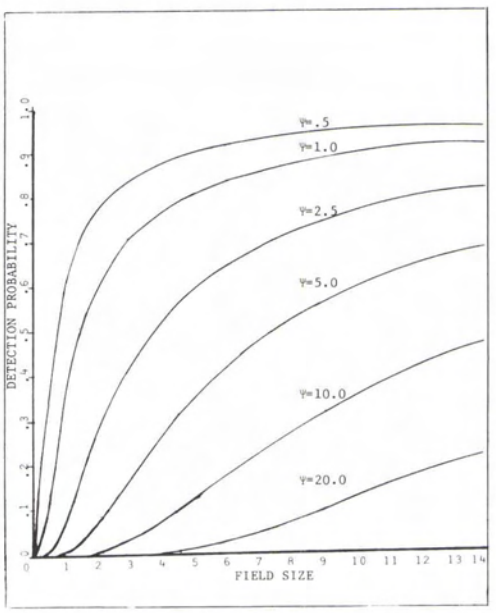

FIG. 6. An illustration of the extreme value detection model as a function of ψ.

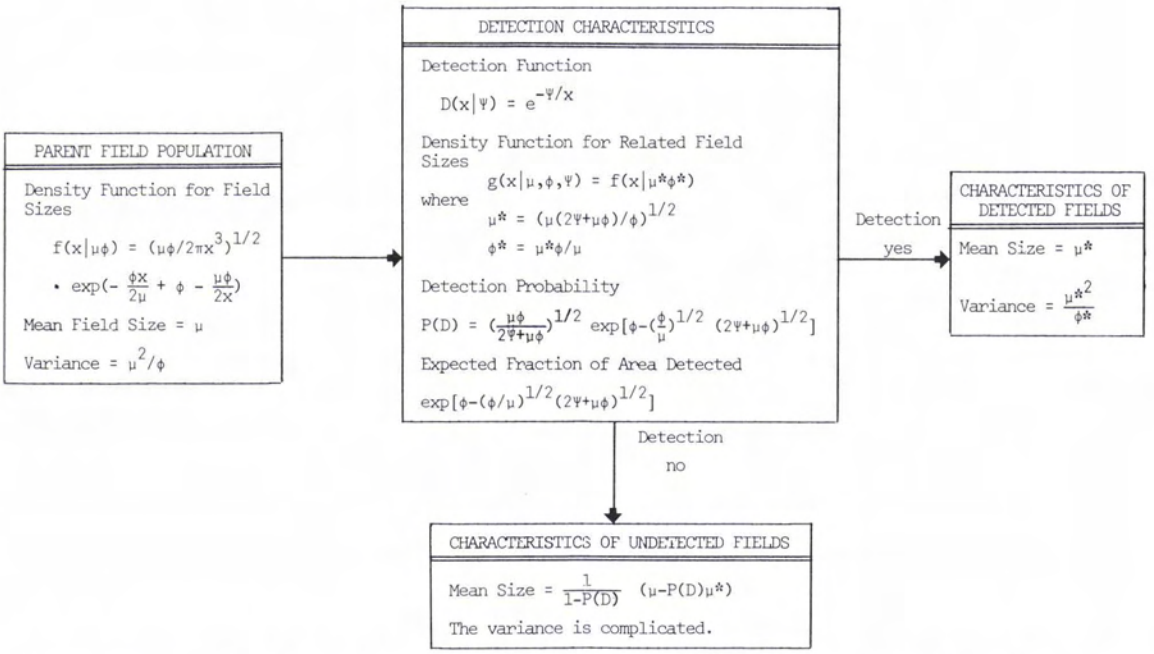

FIG. 7. Summary of analytical result: inverse gaussian field size with "extreme valued distribution" detection.

Note also that it is not possible to estimate all three parameters from the aerial survey data alone. Some additional ground truth data are needed. This is because the maximum likelihood estimates solve the two equations,

$$\bar{x}^2 = \mu/\phi\ (2\psi + \mu\phi) \tag{22}$$

and

$$\left((\sum 1/x_i)/n - 1/\bar{x}\right) = (2\psi + \mu\phi)^{-1}. \tag{23}$$

Only two of the three parameters can be estimated uniquely, although the ratio μ/ϕ can always be determined. That is, by multiplying Equation 23 by 22, the result is

$$\mu/\phi = \bar{x}^2 \cdot \left((\sum 1/x_i)/n - 1/\bar{x}\right). \tag{24}$$

This result can be better understood by noting that the density function (Equation 17), for larger fields, is dominated by the term $\phi x/\mu$. Since large fields are almost always detected, the aerial survey data should reflect this ratio directly, as Equation 24 above indicates.

For the case of cookie cutter detection and an inverse gaussian population, the reader is directed to the work of Patel (1965). With minor adjustments to interpretation, these results are directly applicable to size dependent detection.

An Example Using the Inverse Gaussian Distribution

Data from a study by Podwysocki (1976) will be analyzed to illustrate the foregoing models. In this study, the distribution of field sizes for various major grain producing countries were empirically estimated from fields detected on Landsat imagery. Nearly all these distributions were highly peaked and skewed toward small sizes. Podwysocki used Poisson and log-normal distributions to estimate the number of fields with sizes below or approaching present Landsat resolution limits. However, in his analysis the bias introduced by the undetected smaller fields was not discussed, perhaps because it was considered small.

Figure 8 presents the empirical distribution of the areas of 147 grain fields detected on Landsat imagery in one sample region in Kansas. The mean size of these fields was calculated to be 13.78 ha with a standard deviation of 10.77. This study actually gives conflicting values for the above estimates (q.v., its Figure 5a with its Table 2), but this does not affect the results to follow. The log-normal distribution was found to fit this data extremely well ($\chi^2 = 3.28$ with 16 degrees of freedom). But, as can be observed in Figure 8, the inverse gaussian fits the data nearly as well ($\chi^2 = 5.32$ with 10 degrees of freedom) with parameter estimates

$$\hat{\mu}^* = 13.795, \tag{25}$$

$$\hat{\phi}^* = 1.64. \tag{26}$$

The mode of this distribution is calculated, from the equation in Table 5, to be 6.078 hectares.

Landsat imagery is of limited resolution and

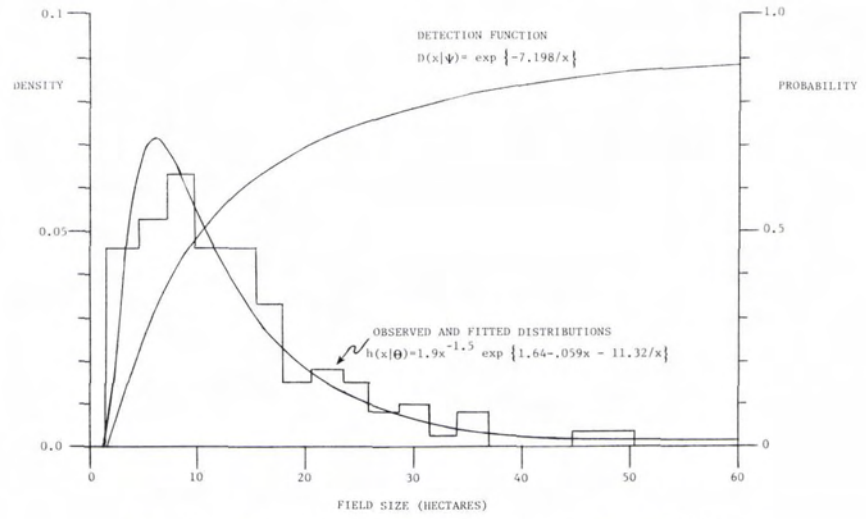

FIG. 8. Distribution of detected Kansas agricultural fields.

consequently small fields, if present, will not be detected. In order to ascertain the extent of this problem some form of ground truth is needed. In a paper by Pitts and Badhuer (1980), sizes of agricultural fields were measured in a ground truth survey from 10 midwestern states. Because this survey included various crops from several regions within the United States, comparability with the survey conducted by Podwysocki is not exact. However, as this example is designed simply to be illustrative, it will be assumed (initially) that the ground truth distribution for all fields from this report approximates the parent distribution underlying Podwysocki's survey. Pitts and Badhuer do not give the mean and variance of this distribution, but they do indicate that the mode is equal to 2.5 ha. This ground truth is sufficient to permit all three parameters of the model to be estimated uniquely.

Assuming the probability of detecting a field on Landsat imagery is given by the extreme value distribution (Equation 18), then this detection function must shift the mode from 2.5 ha to 6.07 ha. Substituting this value into the equation for the mode on Table 5 enables calculation of the parameter ϕ after rearrangement. From the relation $\mu/\phi = \mu^*/\phi^*$, μ can be calculated. Finally, rearranging Equation 19 enables the value of ψ to be calculated from μ^*, μ, and ϕ. This sequence of steps results in values of 7.190 for the detection parameter ψ and $\mu = 8.327$ and $\phi = 0.9899$ for the parent distribution parameters. The "best fit" detection function is also shown in Figure 8.

From Equation 21, the percentage of fields actually detected on the Landsat imagery is estimated to be 31.5 percent. From the equation given in Figure 7, 52.2 percent of the total area is estimated to have been detected. From the best fit detection model (i.e., $\psi = 7.190$), fields about 10 ha in size have a 50 percent chance of being discovered and identified while fields need to be over 50 ha in size to have at least a 90 percent chance of being detected. Though perhaps not impossible, these values seem to be somewhat low. They depend, *inter alia*, upon the assumed mode of the parent distribution. The percentage of fields detected would be greater than indicated above if the mode obtained from ground truth was larger than the assumed 2.5 ha. Figure 9 shows how these percentages vary with the assumed mode of the parent for values between 1 and 6, and indicates the sensitivity of the field and area detection probabilities to this quantity. If the mode of the ground truth distribution were 5 ha, for example, then Landsat imagery would permit detection of about 70 percent of the fields and 85 percent of the area. From the graphs presented in Pitts and Badhuer (1980) 5 ha appears closer to the mode of the distribution of spring wheat including strip fallow fields, perhaps a better match for Podwysocki's "grain fields." If so, probabilities computed on this assumption are more accurate and, in any event, are more plausible. Figure 10 shows the changes in the estimated parent distribution for various assumed values of the mode. Were this an actual analysis rather than merely an illustration, the ground truth data would have been more carefully analyzed,

- to test the fit of the inverse gaussian to the size distribution of fields in the ground truth sample;
- to compute other summary statistics, e.g., μ and ϕ, of the parent population rather than the mode alone;
- to estimate the parameter(s) and test the adequacy of the extreme value detection function; and, finally,

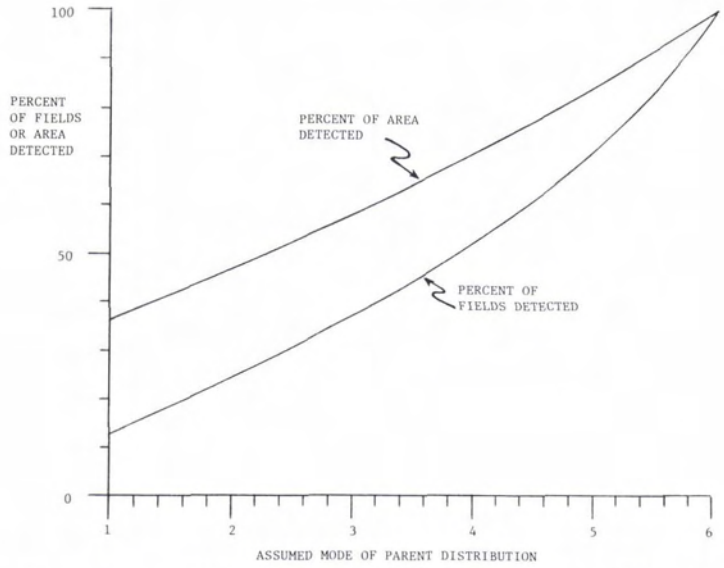

FIG. 9. Percent fields detected and total area as a function of the mode of the parent distribution.

- to estimate the non size-dependent portion of the detection probability.

Nonetheless, the example shows how even limited exogenous ground truth can be used by the methodology for estimation purposes.

GENERALIZATIONS

The analytical results obtained for the exponential parent/exponential detection model can be replicated for the gamma parent/exponential detection model if the threshold parameter, c, in the detection function is zero. If c is greater than zero, then a closed form solution for the detection probability, Equation 2, does not generally exist, and numerical methods must be employed. With access to a computer and programs that can determine constrained maximum likelihood estimates, almost any parent distribution/detection function combination can be utilized to model aerial survey data.

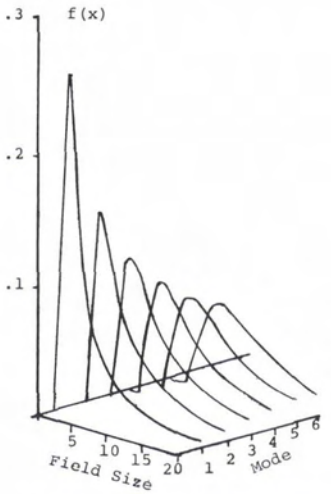

FIG. 10. Parent inverse gaussian distribution for agricultural field sizes for various assumed values of the mode.

It is important to emphasize that, if an aerial survey is analyzed with such models without the guidance of a ground truth sample, then the results must be examined *very* carefully, a point underscored by the Landsat example. It is our experience that several different parent distribution/detection function combinations may fit the aerial survey data well, but unfortunately the estimated detection probability, $P(D)$, can vary appreciably among these alternatives. Moreover, ground truth data are important to a study of the non size-dependent portion of the detection probability. It is possible to have a perfect fit to the distribution of discovered fields and still err by this scalar. A ground truth sample which permits discrimination between possible parent distributions, detection functions, and non size-dependent effects is essential to reduce the uncertainty associated with this scale up factor.

In a broader context, models developed here can also be employed to analyze data where detection may be a monotonic function of variables other than size. For example, in some surveys, the objects of interest may be detectable for only a short period of time. Those objects that remain in this state the longest will have a greater likelihood

of being imaged, depending, of course, on the imaging schedule. Such circumstances might be termed time-dependent detection. Other possibilities are easily imagined.

Concluding Remarks

Three basic approaches for dealing with size-dependent detection have been outlined and illustrated here. Of these, the parametric size-dependent approach has been explored in the most detail, partly because of its novelty but largely because of its power and versatility. Though considerable mathematical manipulation (probably requiring computer use) is required, the approach offers several advantages. Chief among these is the ability to extract the maximum information from limited amounts of ground truth data. As well, this approach is robust to shifts in the parameters of the parent population, changes that could invalidate or alter the calibration between imagery interpretation and ground truth.

Acknowledgments

The authors would like to thank Ms. Mary Kennedy and Ms. Nancy David for helpful discussions and Dr. Paul Saunders for computational assistance. As usual, the reviewers offered useful suggestions to lend clarity and otherwise improve the manuscript.

References

Aldrich, R. C., 1975. Detecting Disturbances in a Forest Environment, *Photogrammetric Engineering and Remote Sensing*, Vol. 41, pp. 39-48.

Ashley, M. D., 1979. Spruce Budworm Damage Evaluation Using Aerial Photographs, *Photogrammetric Engineering and Remote Sensing*, Vol. 42, pp. 1265-1272.

Bauer, M. E., J. E. Cipra, P. E. Anuta, and J. B. Etheridge, 1979. Identification and Area Estimation of Agricultural Crops by Computer Classification of Landsat MSS Data, *Remote Sensing of Environment*, Vol. 8, pp. 77-92.

Berkson, J., 1955. "Maximum Likelihood and Minimum χ^2 Estimates of the Logistic Function, *J. Amer. Statistics Assoc.*, Vol. 50, pp. 130-162.

Bernstein, D., 1974. Are Reforestation Surveys with Aerial Photography Practical?, *Photogrammetric Engineering and Remote Sensing*, Vol. 40, pp. 69-73.

Cropper, P. F., 1980. Errors Incurred in Estimating an Area of Uniform Land Cover Using Landsat, *Photogrammetric Engineering and Remote Sensing*, Vol. 46, pp. 1295-1301.

Cox, D. R., 1970. *Analysis of Binary Data*, Metheun & Co, London.

Estes, J. E., *et al.*, 1975. Fundamentals of Image Interpretation, Chapter 14 of *Manual of Remote Sensing*, Vol. II, American Society of Photogrammetry, Falls Church, Virginia, pp. 1037 *et seq.*

Gilmer, D. S., E. A. Work, J. E. Colwell, and D. L. Rebel, 1980. Enumeration of Prairie Wetlands with Landsat and Aircraft Data, *Photogrammetric Engineering and Remote Sensing*, Vol. 46, pp. 631-634.

Golub, A., and F. E. Grubbs, 1956. Analysis of Sensitivity Experiments when the Level of Stimulus Cannot be Controlled, *J. Amer. Statistical Assoc.*, pp. 257-265.

Hartmann, William K., 1977. Cratering in the Solar System, *Scientific American*, pp. 84-99.

Johnson, N. L., and S. Kotz, 1970. *Continuous Univariate Distribution*, Vol. 1 and 2., Houghton Mifflin Comp., Boston.

Langlie, H. J., 1962. *A Reliability Test Method for 'One Shot' Items*, Aeronautronics Division of Ford Motor Co., Publication No. U-1792.

Maxim, L. D., 1973. *Experimental Design in Sensitivity Testing: The Exponential Model*, Ph.D. Thesis, New York University, School of Engineering and Science.

Maxim, L. D., L. Harrington, and M. Kennedy, 1981a. A Capture-Recapture Approach for Estimation of Detection Probabilities in Aerial Surveys, *Photogrammetric Engineering and Remote Sensing*, Vol. 47, pp. 779-788.

Maxim, L. D., H. D. Weed, L. Harrington, and M. Kennedy, 1981b. Intensity Versus Extent of Coverage, *Photogrammetric Engineering and Remote Sensing*, Vol. 47, pp. 789-800.

Maxim, L. D., L. Harrington, and M. Kennedy, 1981c. Alternative 'Scale Up' Estimators for Aerial Surveys where both Detection and Classification Errors Exist, *Photogrammetric Engineering and Remote Sensing*, Vol. 47, pp. 1227-1239.

Patel, R. C., 1965. Estimates of Parameters of Truncated Inverse Gaussian Distribution, *Annals of the Institute of Statistical Mathematics*, Tokyo, 17, pp. 29-33.

Pitts, D., and G. Badhwar, 1980. Field Size, Length and Width Distribution based on LACIE Ground Truth Data, *Remote Sensing of Environment*, Vol. 10, pp. 201-213.

Podwysocki, M. H., 1976. *An Estimate of Field Size Distributions for Selected Sites in the Major Grain Producing Countries*, Goddard Space Flight Center, X-923-76-93, Greenbelt, Maryland.

Roswell, C. Written communication cited in Estes, *et al.* (q.v.).

Tweedie, M. C., 1957a. Statistical Properties of Inverse Gaussian Distributions I, *Annals of Mathematical Statistics*, Vol. 28, pp. 362-377.

———, 1957b. Statistical Properties of Inverse Gaussian Distributions II, *Annals of Mathematical Statistics*, Vol. 28, pp. 696-705.

Wilde, D. W., 1963. *Optimum Seeking Methods*, Prentice Hall, Englewood Cliffs, New Jersey.

Work, E. A., and D. S. Gilmer, 1976. Utilization of Satellite Data for Inventoring Prairie Ponds and Lakes, *Photogrammetric Engineering and Remote Sensing*, Vol. 42, pp. 685-694.

(Received 31 July 1981; accepted 6 December 1981; revised 14 February 1982)

Appendix
Estimation of the Parameter, Ψ, of the Extreme Value Detection Function

The data for this problem consist of pairs of values, x_i and u_i, from a matched ground truth and imagery interpretation experiment. For each of n fields, subscripted $i = 1, \ldots, n$, the size, x_i, and the imagery observation, u_i, are assumed known. u_i is bivalent; it is defined as 1.0 if the i^{th} field was detected and 0 otherwise. For a fixed value of Ψ, the probability that $u_i = 1.0$, given a field of size x_i, is $\exp[-\Psi/x_i]$. Following the same logic as Langlie (1962) or Golub and Grubbs (1956) for the normal distribution or Maxim (1973) for the exponential distribution, the probability, p_i, of an outcome, u_i, given a field size, x_i, is given by

$$p_i = p(u_i|x_i,\Psi) = u_i\exp(-\Psi/x_i) + (1 - u_i)(1 - \exp(-\Psi/x_i)). \quad \text{(A-1)}$$

The likelihood, L, of the outcome $U = u_i$, $i = 1, \ldots, n$, is given by the product of the probabilities, p_i, or equivalently $\ln L$ is the sum $\ln p_i$. Leaving aside degenerate cases, $u_i = 0$ for all i or $u_i = 1.0$ for all i, and assuming all $x_i > 0$,

$$\ln(p_i) = \frac{-u_i\Psi}{x_i} + (1 - u_i)\ln(1 - e^{-\Psi/x_i}), \quad \text{(A-2)}$$

recalling that u_i can only assume the value 0 or 1.

Now,

$$\frac{\partial \ln L}{\partial \Psi} = \sum_i \frac{\partial \ln p_i}{\partial \Psi}, \quad \text{(A-3)}$$

but

$$\frac{\partial \ln p_i}{\partial \Psi} = \frac{-u_i}{x_i} + \frac{(1 - u_i)e^{-\Psi/x_i}}{x_i(1 - e^{-\Psi/x_i})}. \quad \text{(A-4)}$$

From Equations A-3 and A-4, setting the derivative of Equation A-3 with respect to Ψ equal to zero leads to the transcendental equation,

$$\sum_i \frac{(1 - u_i)e^{-\Psi/x_i}}{x_i(1 - e^{-\Psi/x_i}} - \sum u_i/x_i = 0. \quad \text{(A-5)}$$

Observe that, for a fixed set of fields (x_i) and outcomes (u_i), the LHS of Equation A-5 is monotonic decreasing in Ψ. Denoting the value of the LHS by $S(\Psi)$, Equation A-5 implies a functional relationship between $S(\Psi)$ and Ψ as shown in Figure A-1. Highly efficient numerical root finding algorithms have been devised. In particular, a binary search technique termed Bolzano's Method (Wilde, 1963) can be employed. In essence, Bolzano's Method operates by evaluating the function at midpoints (Ψ_m) of successive intervals of uncertainty (Ψ_ℓ, Ψ_h). If the value of the function is positive (negative), the new left (right) endpoint is set equal to the midpoint of the previous interval. The procedure can terminate whenever one of a number of alternative stopping criteria are satisfied. The most common stopping criteria are

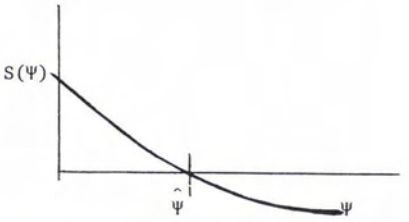

Fig. A-1. The functional relationship between $S(\psi)$ and ψ as implied from Equation A-5.

(i) $S(\Psi) < \epsilon$, or
(ii) $\Psi_h - \Psi_\ell < \epsilon'$

where ϵ is an arbitrarily small convergence bound.

Example

Table A-1 shows results of an imagery and ground truth experiment.

The results of Bolzano search assuming Ψ is between 0.5 and 15 are shown in Table A-2. In this example the maximum likelihood value of Ψ is 4.58.

For the case where the detection probability is given by $\gamma e^{-\Psi/x}$, i.e., the term γ is used to model the non size-dependent portion of the detection process, the maximum likelihood estimates $\hat{\Psi}$ and $\hat{\gamma}$ can be obtained by solving the pair of equations,

$$\sum \frac{(1 - u_i)\gamma e^{-\Psi/x_i}}{x_i(1 - \gamma e^{-\Psi/x_i}} - \sum \frac{u_i}{x_i} = 0, \quad \text{(A-6)}$$

and

$$\frac{1}{\gamma}\sum u_i - \sum \frac{(1 - u_i)e^{-\Psi/x_i}}{(1 - \gamma e^{-\Psi/x_i})} = 0. \quad \text{(A-7)}$$

Determining an Optimal Ground Truth Collection Sample

The asymptotic variance of the maximum likelihood estimate, just determined numerically, can be calculated using the well known result,

$$\text{Var}(\hat{\Psi}) = \left[-E\left(\frac{\partial^2 \ln L}{\partial \Psi^2} \right) \right]^{-1}. \quad \text{(A-6)}$$

Table A-1. Results of an Imagery and Ground Truth Experiment

Field Size (arbitrary units, x_i)	Detection Outcome, u_i
10	1
2	0
10	0
2	0
8	1
14	1
1	0
7	1
6	0

TABLE A-2. RESULTS OF A BOLZANO SEARCH ASSUMING ψ IS BETWEEN 0.5 and 15.

ψ Assumed	$S(\psi)$
7.750	−0.269074
4.125	+0.087212
5.9375	−0.160538
5.0313	−0.064925
4.5781	−0.001714

One criterion for determining an optimal ground truth sample is to choose field sizes which minimize this asymptotic variance. For the extreme value distribution, the above expression can be evaluated by differentiating Equation A-4 a second time and then summing over i, or

$$\frac{\partial^2 \ln(P_i)}{\partial \Psi^2} = \frac{-(1-u_i)e^{-\Psi/x_i}}{x_i^2(1-e^{-\Psi/x_i})^2}.$$

Now,

$$E(1-u_i) = 1 - e^{\Psi/x_i},$$

so,

$$\mathrm{Var}(\hat{\Psi}) = \left[-E\left(\sum_{i=1}^{n} \frac{\partial^2 \ln p_i}{\partial \Psi^2} \right) \right]^{-1},$$

$$= \left[\sum_{i=1}^{n} \frac{e^{-\Psi/x_i}}{x_i^2(1-e^{-\Psi/x_i})} \right]^{-1}. \quad \text{(A-9)}$$

To determine those field sizes, x_i, that minimize this asymptotic variance, the reciprocal of Equation A-9 can be maximized with respect to each x_i, because the denominator is always nonnegative. Differentiating this reciprocal, the result is

$$\frac{\partial(\mathrm{Var}\,\hat{\Psi})^{-1}}{\partial x_i} = \frac{e^{-\Psi/x_i}\left[\Psi - \Psi e^{\Psi/x_i} - 2x_i(1-e^{-\Psi/x_i}) + \Psi e^{-\Psi/x_i}\right]}{x_i^4(1-e^{-\Psi/x_i})^2}$$

Setting this to zero then gives the equation,

$$\Psi - 2x_i(1-e^{-\Psi/x_i}) = 0,$$

or

$$e^{-\Psi/x_i} = 1 - \frac{\Psi}{2x_i}. \quad \text{(A-10)}$$

This equation has solutions at x_i equal to infinity and

$$x_i = \Psi/1.594. \quad \text{(A-11)}$$

It can be shown that the value of x_i given in Equation A-11 minimizes $\mathrm{Var}(\hat{\Psi})$ with respect to x_i. Thus, the optimal ground truth sample would be to select fields each of size $\Psi/1.594$. Note that fields of this size have a detection probability of

$$D(x/\Psi) = e^{-\Psi/x_i} = e^{-1.594} \cong 0.203.$$

The optimal sampling plan cannot be applied exactly because it requires knowledge of the unknown ψ. Given even a rough estimate of Ψ, however, the above results offer useful insight as to how the ground truth sample ought to be collected.

Reviewers Needed

Reviewers are needed for *Photogrammetric Engineering and Remote Sensing* for papers dealing with hydrospherics. Subjects typically involve general hydrology, oceanography, water quality, hydrologic modeling, snow and ice, and wetlands. Competent reviewers maintain the quality of the technical papers, and an adequate list of reviewers reduces the lag time for publication.

Anyone wishing to contribute their time and expertise should contact one of the officers of the Hydrospherics Committee listed below. Please indicate your area of expertise and the number of papers per year you are willing to review.

Dr. Thomas J. Jackson
USDA Hydrology Laboratory
Room 139, Building 007,
BARC-West
Beltsville, Maryland 20705

Dr. Siamak Khorram
North Carolina State University
Department of Electrical
Engineering
P.O. Box 5275
Raleigh, North Carolina 27650

Dr. Thomas Mace
Lockheed, Incorporated
Image Analysis Lab
P.O. Box 15027
Las Vegas, Nevada 90114